



On the Impact of Lacing Reinforcement Arrangement on Reinforced Concrete Deep Beams Performance

Shatha D. Mohammed ^{1*}, Hamza M. Salman ¹, Teghreed H. Ibrahim ¹,
Nazar K. Oukaili ¹, Abbas A. Allawi ¹

¹ Department of Civil Engineering, University of Baghdad, Baghdad 17001, Iraq.

Received 17 November 2024; Revised 18 January 2025; Accepted 24 January 2025; Published 01 February 2025

Abstract

The optimum design is characterized by structural concrete components that can sustain loads well beyond the yielding stage. This is often accomplished by a fulfilled ductility index, which is greatly influenced by the arrangement of the shear reinforcement. The current study investigates the impact of the shear reinforcement arrangement on the structural response of the deep beams using a variety of parameters, including the type of shear reinforcement, the number of lacing bars, and the lacing arrangement pattern. It was found that lacing reinforcement, as opposed to vertical stirrups, enhanced the overall structural response of deep beams, as evidenced by test results showing increases in ultimate loads, yielding, and cracking of 30.6, 20.8, and 100%, respectively. There was also a 53.6% increase in absorbed energy at the ultimate load. The shear reinforcement arrangement had a greater impact and a significant effect on the structural response than the number of lacing bars. For lacing reinforcement with a phase difference equivalent to the half-lacing cycle (i.e., phase lag lacing), the percentage of improvement under different loading stages was 6.7-27.1% and 20.8-113.3%, respectively. The structural responses are significantly impacted by the lacing arrangement; members with two and three lacing bars, respectively, exhibited improvements in ultimate load of 30.6% and 47%. Beyond the yielding stage, the phase lag lacing specimens deviated from those without phase lag lacing and normal shear stirrups because of the lacing contribution. Phase lag specimens showed more strain than specimens without phase lag lacing, meaning that the lacing reinforcement contributed more to the beam strength. It was found that the first shear cracking load of all the laced reinforced specimens was higher than that of the conventional shear stirrup specimens. Phase lag lacing produced the greatest improvement, with two bars achieving 92.44% and three bars achieving 217.07%. For the aforementioned number of bars, lacing shear reinforcement without phase lag was less successful, with 36.91% and 46.53%, respectively.

Keywords: Lacing Reinforcement; Deep Beam; Vertical Stripes; Self-Compacting Concrete; Shear.

1. Introduction

In constructions made of reinforced concrete, beams are components required to sustain transverse loads. Three categories of reinforced concrete beams are distinguished by their shear span to the effective depth ratio (a/d): deep beams ($a/d=1.0$), moderately deep beams ($1.0 < a/d < 2.5$), and ordinary shallow beams ($a/d > 2.5$) [1-4]. Because of their high depth-to-length ratio, deep beams are regarded as two-dimensional members. Consequently, deep beam cross-sections exhibit a nonlinear bending deflection, leading to a nonlinear distribution of strain throughout their sections. Therefore, shear deflection is significant and shear is the governing requirement when designing deep beams as opposed to pure flexural deflection [5-9]. Shear reinforcement is used mostly in concrete structures design to prevent the development and extension of diagonal cracks. Conventional stirrups reinforcement or continuous lacing bars are the

* Corresponding author: shatha.dh@coeng.uobaghdad.edu.iq

<http://dx.doi.org/10.28991/CEJ-2025-011-02-019>



© 2025 by the authors. Licensee C.E.J, Tehran, Iran. This article is an open access article distributed under the terms and conditions of the Creative Commons Attribution (CC-BY) license (<http://creativecommons.org/licenses/by/4.0/>).

two types of transverse reinforcement used in deep concrete beams. Lacing bars are run parallel to the main flexural reinforcement and bent diagonally between flexural reinforcement layers. They are positioned in the principal bending plane and secured there by transverse bars. Many studies and data, especially from statically tested beams, provide the basis of the conventional stirrups reinforcement specifications [10, 11]. The role of lacing reinforcement in beams subjected to monotonic static loads has received very little attention. By better understanding the contributions of lacing and conventional shear reinforcement, the designer will be able to compare and assess the advantages of each type and evaluate which is most appropriate for the structure in concern. By providing the concrete core of the beam with superior confinement [12-14], lacing reinforcement improves the ductility index and offers more shear resistance than conventional stirrups reinforcement, which is crucial for concrete structures [13, 15].

Numerous factors, including reinforcing details, additive materials, and fiber volume percentage, were considered while assessing approaches to improve the structural concrete member ductility index [16–21]. Al-Gasham [22] showed that by replacing steel stirrups with lacings, steel bars bent at angles greater than 30° , the failure mode may be converted to pure flexural. The performance of laced reinforced concrete (LRC) and its utilization in blast-resistant design have been extensively investigated by Lakshmanan [23]. It was found that LRC beams respond to a low shear span-to-depth ratio.

In an experimental study, Allawi & Jabir [24] inspected one-way laced reinforced concrete slabs under static load. Nine slabs were fabricated and tested to investigate the flexural behavior using three parameters: the lacing reinforcement ratio, the reinforcement ratio in the tension zone, and the clear span-to-effective depth ratio. The authors concluded that a continuous lacing bar of 0.0065 ratio resulted in a 57% increase in ultimate load when compared to the control slab without lacing reinforcement. Additionally, a 31.25% decrease in the clear span-to-effective depth ratio resulted in a 103.57% failure load increase. The effect of lacing reinforcement on the one-way concrete slab behavior under monotonic load was examined by Hallawi & Al-Ahmed [25]. Three $1500 \times 600 \times 130$ mm slabs—two with lacing reinforcement and one reference slab without—were tested in a simply supported scheme. Main flexural steel bars with a 0.31% ratio were used for reinforcement of the tested slabs. One slab had a lacing reinforcement ratio of 0.26%, whereas the other slab had a ratio of 0.52%. The test findings demonstrated that, in comparison to the specimen without lacing reinforcement, the cracking load, ultimate load, and ductility index were enhanced by (28, 45, and 33%) and (16, 40, and 49%) for lacing steel ratios of 0.26% and 0.52%, respectively.

In an experimental investigation, six high-strength one-way slabs of reinforced concrete were tested to see how the laced structural members would respond to exposure to fire [26]. The concrete compressive strength ($f_c' \approx 60$ MPa), flexural reinforcement details, and dimensions $2000 \times 750 \times 150$ mm for length, width, and depth were all same across all tested specimens. Three lacing steel ratios—0.0021, 0.0040, and 0.0060—were used in relation to the lacing reinforcement. The six specimens were split up into three pairs, each with the same ratio of lacing steel. Before being tested, one specimen from each pair was subjected to fire for two hours at 500°C . The other three specimens were tested without any fire exposure. To evaluate the flexural behavior of the simply supported slabs under a four-point bending test, two line loads were applied in the middle third of the slabs. The experimental program's results showed that, in comparison to their comparable unexposed to fire specimens, the residual strength of the slabs exposed to fire with lacing steel ratios of 0.0021, 0.004, and 0.006 was 72.56%, 70.54%, and 70.82%, respectively. Furthermore, for the lacing steel ratios under consideration (0.0021, 0.004, and 0.006), an increase in the deflection at failure was found to be 11.34%, 14.67%, and 17.22%, respectively.

Abdullah et al. [27] investigated three reinforced concrete beams of $(2110 \times 400 \times 350)$ mm dimensions with two, three, and four vertical stirrup legs across the beam width while keeping the stirrup contributions in the design equation constant in order to experimentally study the shear failure mechanism of RC beams with various vertical reinforcement configurations. Shear resistance components, strains in vertical stirrup legs, internal cracking patterns, load-displacement correlations, and concrete strain relationships were also investigated. According to the findings, the shear strength of the RC beams is improved and internal crack formation is successfully limited when two equally spaced internal vertical stirrup legs are used with conventional closed stirrups. The structural performance of laced reinforced concrete beams under reverse cyclic stress was compared to that of ordinary reinforced concrete beams by Johnson et al. [28]. Two cantilever beams with dimensions of $660 \times 300 \times 300$ mm with adequate flexural reinforcement (4 $\phi 12$ mm for top and bottom reinforcement) were tested as part of the experimental program. The first specimen's shear reinforcement was a 45° inclined lacing steel bar, and the second specimen had vertical closed stirrups. The tested specimens had the same shear reinforcement diameter and spacing. Even at large displacements, laced reinforced beams had superior crack resistance, whereas conventional beams were subject to diagonal tension cracks and vertical cracks. Conventional beams cracked under lower applied loads and experienced low ductility. Contrarily, laced beams showed better energy absorption as evidenced by their increased energy dissipation. Furthermore, laced beams were noticeably stiffer.

In their assessment of several works on modifying shear reinforcement in beams, Bello & Dela Cruz [29] focused on geometry, inclination, and spacing. Results indicate that RC beams with truss and spiral reinforcement induce deflections between 80 and 150 mm and enhance flexural and shear capacities by 18.148% and 13.08%, respectively.

Because of these difficulties, the researchers advise developing complicated models and assessing structural members using the Finite Element Method (FEM). This will save money and effort and yield accurate, safe outcomes.

An analytical research by Bello et al. [30] used ABAQUS software to examine reinforced concrete beams with variable shear reinforcement. 17 finite element models, including four beams each with a different shear reinforcement scheme (rectangular spiral, rectangular truss, vertical X-shape, and X-shaped truss system) and one control beam. Four different spacings were also taken into consideration for each shear reinforcement system, primarily 75, 100, 125, and 150 mm, in order to assess the flexural capacity, ductility, failure mechanisms, crack patterns, and load-deflection relationship. According to the results, the rectangular truss system significantly improved the performance of the reinforced concrete beams, particularly at 100 mm spacing. Furthermore, beam performance was greatly impacted by shear reinforcement inclination and spacing, which varied depending on their arrangement.

2. Research Methodology

The primary goal of this study is to investigate the effects of the lacing reinforcement arrangement on the structural performance of deep beams and identify its benefits above nominal shear reinforcement. The research methodology comprised experimental and numerical parts. The materials, fabrication, and testing of the experimental specimen were all included in the experimental part. Using ABAQUS software, numerical finite element analysis was performed in the second section. This included model development, model validation, and parameter analysis. Figure 1 shows the details of the research methodology.

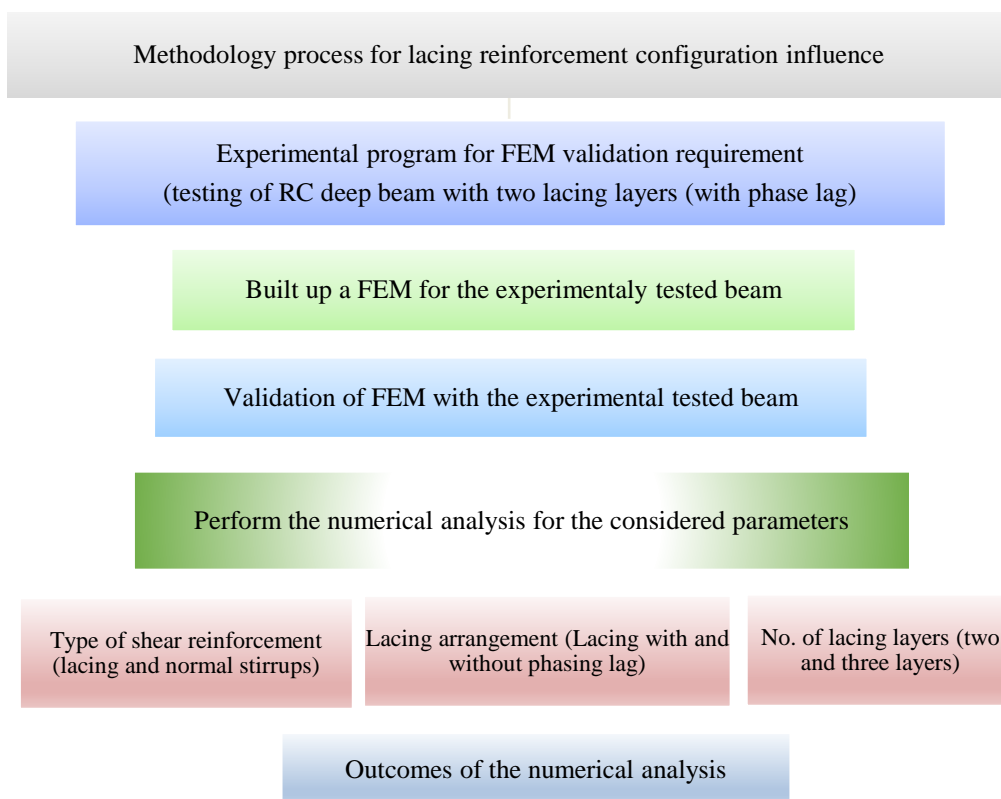


Figure 1. Research Methodology

3. Experimental Program

3.1. Constitutive Materials

The investigated specimens were cast using self-compacting concrete (SCC), which primarily used ordinary Portland cement OPC (CEM I-42.5 N), crushed nominal size (10) mm coarse aggregate, fine aggregate, silica fume (SF), water, and superplasticizer (SP). According to I.Q.S. 5/2019 [31], cement was tested; its chemical and physical properties are shown in Tables 1 and 2, respectively. The physical, chemical, and sieving characteristics of the coarse and fine aggregate are presented in Tables 3 and 4, which comply with IQS No. 45/1984 [32]. With an accelerated pozzolanic strength activity index of 112% at 7 days, ISOMAT silica fume was utilized in this investigation. It conformed to ASTM C1240-20 [33]. Superplasticizer SikaViscoCrete-5930 was added to the concrete mix to provide SCC for all specimens, meeting ASTM C494/C494M-17 [34] type (F).

Table 1. Cement chemical composition

Chemical Composition	Result	Limits of IQS No. 5/2019 (42.5N)
Lime – CaO	63.2	-----
Silica - SiO ₂	22.1	-----
Alumina - Al ₂ O ₃	4.68	-----
Iron Oxide - Fe ₂ O ₃	2.54	-----
Magnesia (MgO)	3.22	5.0 (max)
Sulfate - SO ₃	2.15	≤ 2.8 If C3A > 3.5
Insoluble residue - I.R	0.89	1.5 (max)
Loss on Ignition - L.O.I	1.99	4.0 (max)
<i>The Main Compound of OPC</i>		
Tri Calcium Silicate (C3S)	54.20	-----
Di Calcium Silicate (C2S)	22.48	-----
Tri Calcium Aluminate (C3A)	8.11	-----
Tetra Calcium Aluminate Ferrite (C4AF)	7.73	-----

Table 2. Cement physical properties

Physical Properties	Result	Limits of IQS No.5/2019
Specific surface area m ² /kg (Blain method)	326	≥ 250
Initial setting time, (min)	125	≥ 45
Final setting time, (hr.: min)	4:49	≤ 10
Compressive strength, (MPa) @ 2 days	17	≥ 10
@ 28 days	43.2	≥ 42.5

Table 3. Coarse aggregate characteristics

Sieve size (mm)	Passing %	Limits of IQS No. 45/1984 Nominal size (10) mm
20	100	100
14	100	100
10	95	85-100
5	17	0-25
2.36	2	0-5
Property	Test Result	Limits of IQS No. 45/1984
Specific gravity	2.59	-----
Absorption	0.8%	-----
Sulfate content (SO ₃)	0.07%	≤ 0.1%
Dry-rodded density	1598 kg/m ³	-----

Table 4. Fine aggregate characteristics

Sieve size (mm)	Passing %	Limits of IQS No. 45/1984 - Zone 2
10	100	100
4.75	96	90-100
2.36	83	75-100
1.18	67	55-90
0.6	41	35-59
0.3	20	8-30
0.15	4	0-10
Property	Test Result	Limits of IQS No. 45/1984
Specific gravity	2.56	----
Absorption	0.89%	----
Dry rodded density	1629 kg/m ³	----
Sulfate content (SO ₃)	0.41%	0.5% (max)
Fine particles passing from the sieve 75 μm	2.78%	5.0% (max)

The tested beams in various zones were reinforced with mild steel. Steel bars of two different diameters were employed, namely 10 mm bars for flexural reinforcement and 8 mm bars for shear reinforcement. Table 5 displays the steel reinforcement test results. The steel's properties were found to be compliant with ASTM A615M [35].

Table 5. Steel reinforcement test outcomes

No.	Diameter (mm)	Sectional area (mm ²)	Yield Strength (MPa)	Ultimate Strength (MPa)	Elongation (%)
1	10.0	76.06	630.0	685	11.2
2	8.0	50.28	580.0	620	11.9

3.2. Mix Design and Fresh Properties of Self-Compacting Concrete

By considering the mix proportions shown in Table 6, the target concrete compressive strength (45 MPa) was attained. To select suitable mix proportions for satisfying the fresh self-compacting concrete (SCC) requirement and the estimated compressive strength, a number of trials were conducted. Five tests were conducted to evaluate the properties of the fresh SCC mix, as indicated in Table 7. Each of the five tests—slump flow, T500mm, V- funnel, L-box (H₂/H₁), and segregation index (SI) percentage—was within the ranges of EFNARC 2005 [36].

Table 6. Mix proportions of SCC

Cement (kg/m ³)	Fine aggregate (kg/m ³)	Coarse aggregate (kg/m ³)	Water (l/m ³)	SF (kg/m ³)	SP (l/m ³)
431.2	680	950	185	8.8	13.2

Table 7. Fresh properties of SCC

Mix	Fresh properties test				
	Slump flow (mm)	T _{500mm} (sec)	V- funnel (sec)	L-box (H ₂ /H ₁)	Segregation index (%)
SCC	730	2.8	6.5	0.91	15.3
(EFNARC 2005)	SF1 550 - 650 SF2 660 - 750	VS1 ≤ 2	VF1 ≤ 8	≥ 0.8	SR1 ≤ 20
Limits	SF3 760 - 850	VS2 > 2	VF2 (9 - 25)		SR2 ≤ 15

3.3. Characteristics of the Tested Specimen

The rectangular section of the tested beam was 250 mm deep by 200 mm wide, with total and clear spans of 1500 mm and 1300 mm, respectively. The beam was exposed to monotonic static load in simply supported scheme where the roller and pin supports were placed 100 mm apart from the edge of the specimen. Figure 2 shows details of the applied load and support positions that correspond to the two-point supporting beam. The top and bottom zones of the tested beam included longitudinal reinforcements in the form of two φ10 mm steel bars. On both sides of the beam, two layers of lacing reinforcement were used as shear reinforcement. The two lacing layers were separated by a phase lag of 210 mm, or half a lacing cycle. The hardened properties of the SCC are displayed in Table 8.

Table 8. Mechanical proportions of the hardened SCC

Compressive strength (f'_c), MPa	Splitting tensile strength (f_t), MPa	Modulus of elasticity (E_c), MPa
45.6	4.0	31050

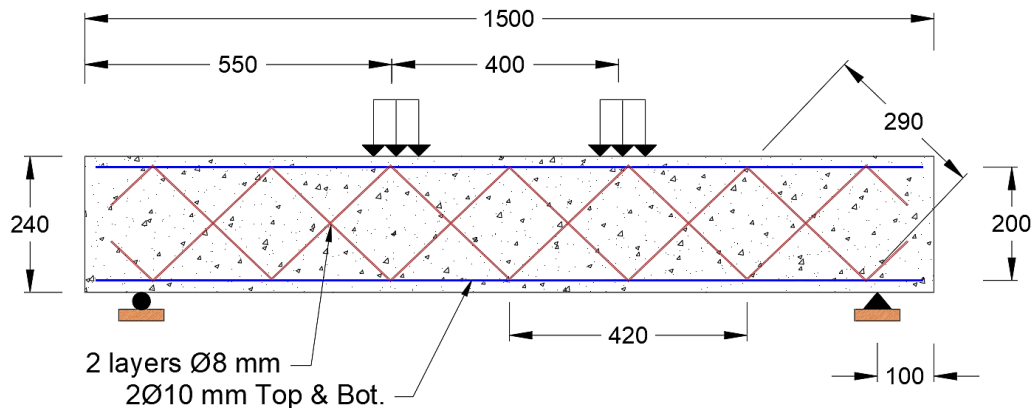


Figure 2. Tested specimen details (all dimensions are in mm)

3.4. Test Technique

The experimental test procedure was divided into many stages. The specimen was painted white to allow for greater crack viewing, and then it was placed on hemispherical supports that were designed to act as simple supports. The static load was applied and measured using a 100-ton hydraulic jack and a 200-ton load cell. Since the static load was applied using a two-point load arrangement, an I-section steel girder was considered to evenly distribute the load between two locations that were 400 mm apart. A linear variable differential transformer (LVDT) with a stroke length of 10 cm was used to measure the vertical deflection at mid span of the tested specimen. The arrangement of the test setup and the instrumentation used are shown in Figure 3. A load step of 10.0 kN was used in the test, and the applied load was increased progressively until failure. The development and progress of cracks was precisely monitored and recorded at each increment. A computerized system automatically documented the test results, including the vertical deflection and the applied load.

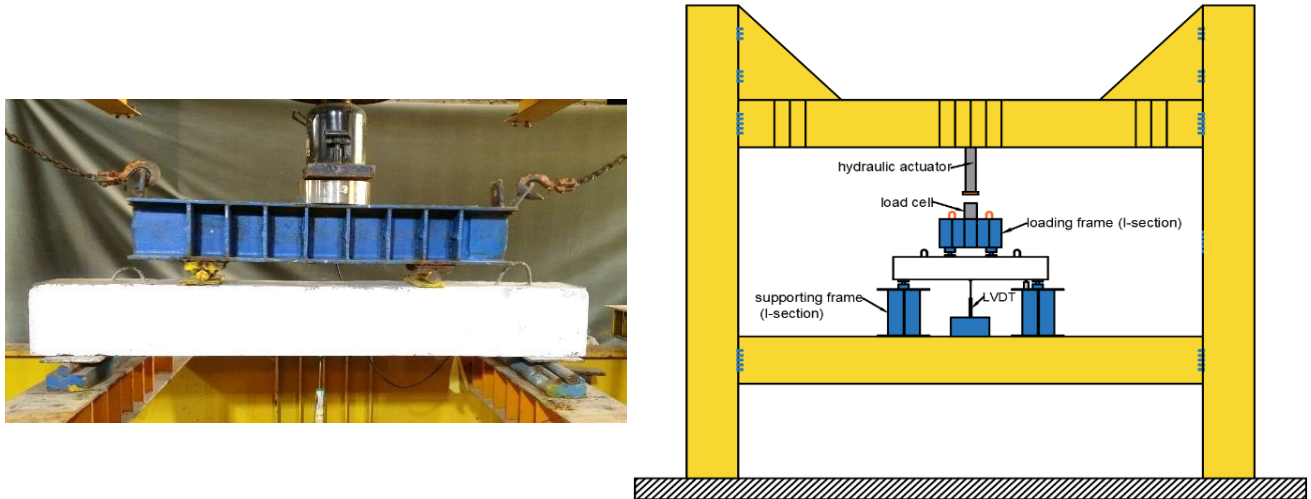


Figure 3. Experimental test arrangement

4. Finite Element Modeling

The most efficient method for analyzing and predicting the behavior of laced reinforced concrete beams is the Finite Element Method. ABAQUS/CAE 2017 software was used to develop the Finite Element (FE) model, which accurately predicts the behavior of laced reinforced concrete beams. The study took into account the interface aspect, the non-linear behavior of the concrete and reinforcing bars, and the geometric effects associated with second-order analysis.

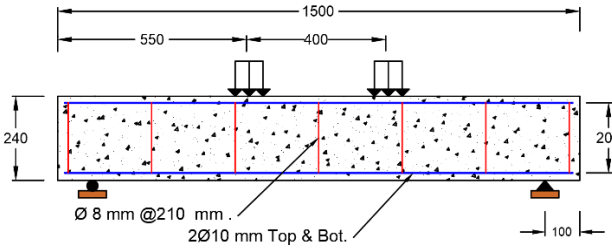
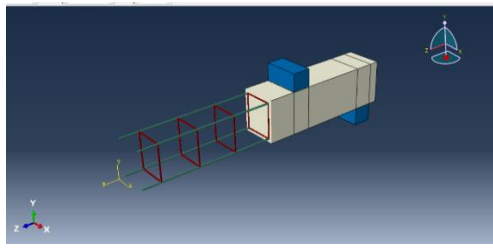
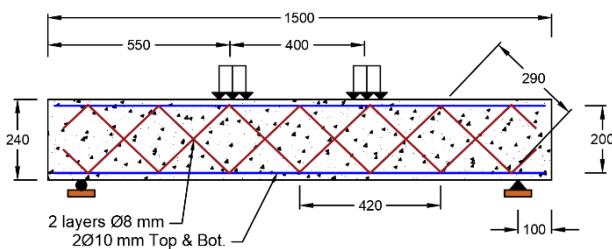
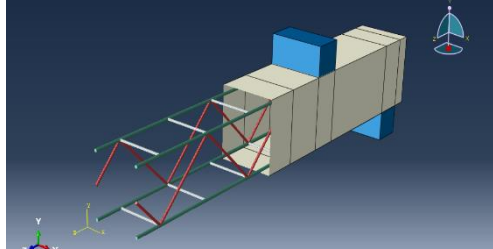
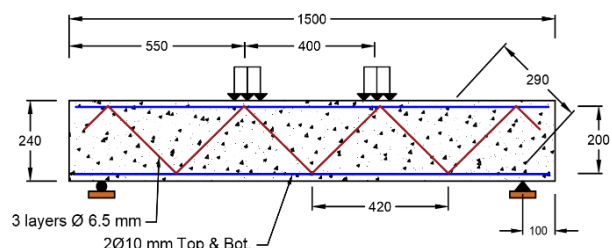
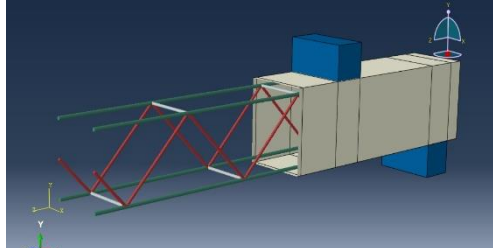
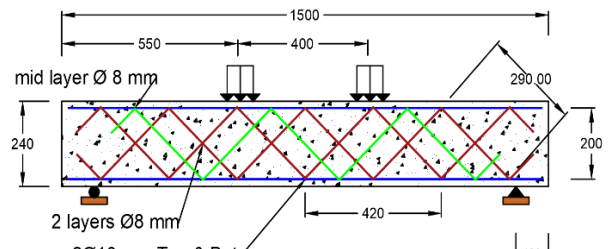
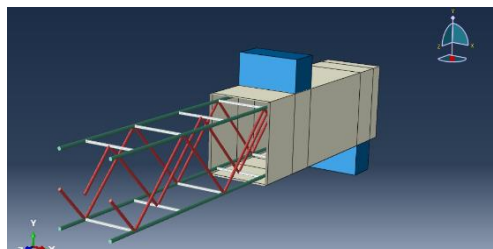
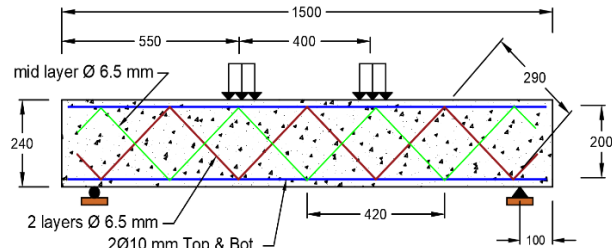
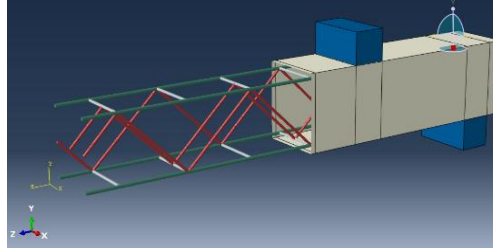
4.1. The Adopted Lacing Arrangements

In addition to the ordinary vertical stirrups, four lacing arrangements of the transverse reinforcement were adopted in the numerical experiment to determine their impact on the behavior of laced RC beams. In the first specimen (BNS), two-legged steel stirrups measuring 8 mm @ 210 mm were taken into consideration as shear reinforcement.

Two lacing bars with 8 mm diameter one on each beam side with a phase difference equal to half-lacing cycle defined the arrangement in the second specimen (BL2D). No change in the phase of the two lacing bars was considered, even though the arrangement in the third specimen (BL2S) was comparable to that in the third specimen (BL2D).

To make the total lacing bar area of three bars equal to the total lacing bar area of two bars of 8 mm diameter, the number of lacing bars was increased to three in the fourth specimen (BL2S1D) from two, and the bar diameter was decreased to 6.5 mm. The arrangement in specimen (BL2S1D) is defined by two 6.5 mm diameter lacing bars, one on either side of the beam with no phase change and a third inserted halfway across the width of the beam cross-section between them with a phase difference equal to half-lacing cycle. Three 6.5 mm diameter lacing bars, one on each side of the beam and the third positioned midway across the breadth of the beam cross-section between them, define the arrangement in the fifth specimen (BL3S). The three bars did not undergo any phase changes. Table 9 displays the geometric layout and details for each specimen under consideration.

Table 9. Shear reinforcement arrangement in the numerical experiment

Specimen designation	Specimen details	Numerical Modeling
BNS		
BL2D		
BL2S		
BL2S1D		
BL3S		

4.2. Elements of the Developed Model

Hexahedral elements of eight nodes with three degrees of freedom each and reduced integration (C3D8R) were used to simulate every component of this investigation, with the exception of the longitudinal and shear reinforcement. However, a two-node linear shear-flexible beam in space elements with three degrees of freedom for each node was employed to model the reinforcing components (B31).

4.3. Boundary Condition and Load Application

The structure model's responses are being greatly regulated by the boundary conditions that have been implemented. Simply supported boundary conditions (also known as hinge-roller) were used in this investigation. However, problems with convergence may occur when the nonlinear analysis is validated, especially when cracks start to appear. In order to prevent a convergence issue, a suitably short time increment (load increment) was used. Performing this, the

convergence issue is improved and the analysis is guaranteed to follow the load-deflection curve. The time increment that was chosen was 10% of the time period. Furthermore, a constant maximum limit of time increment was used and set to 0.1 periods. A rigid steel plate (high stiffness plate) was subjected to a pressure distribution that represented the applied load, see Figure 4.

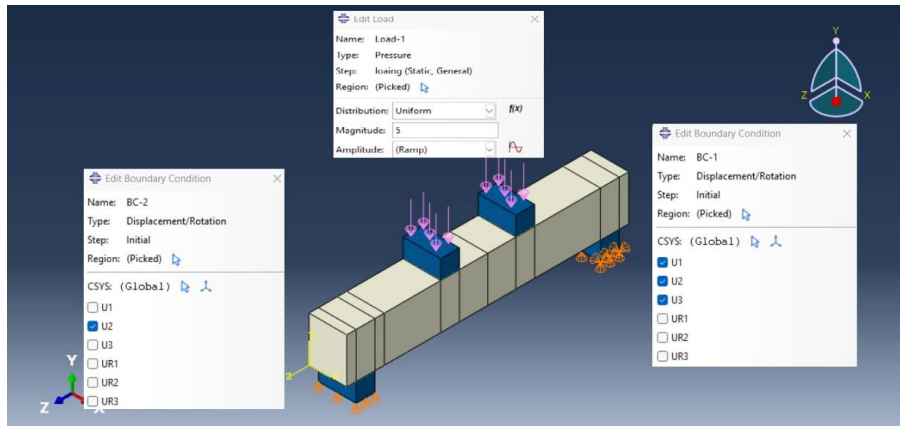


Figure 4. Adopted boundary conditions and applied load in the numerical experiment

4.4. Materials Properties

Concrete damage plasticity (CDP) model has been used successfully for predicting the standard concrete test response in both tension and compression, Coronado and Lopez [37]. Characterizing the CDP model required defining the concrete modulus of elasticity, Poisson’s ratio, and damage plasticity parameters. Moreover, concrete behavior in both compression and tension must be provided, see Figure 5.

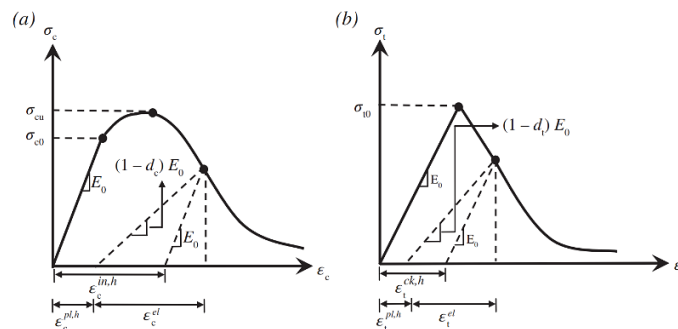


Figure 5. Concrete behavior in both compression (a) and tension (b) [37]

To identify the concrete uniaxial compressive behavior, two approaches can be used: experimental tests or existing constitutive models. For instance, Kent & Park [38] have proposed constitutive models for unconfined concrete, see Figure 6. This model can be expressed by the following expression:

$$\sigma_c = \sigma_{cu} \left[2 \left(\frac{\epsilon_c}{\epsilon'_c} \right) - \left(\frac{\epsilon_c}{\epsilon'_c} \right)^2 \right] \tag{1}$$

where σ_c and ϵ_c are the nominal compressive stress and strain, respectively. σ_{cu} and ϵ'_c are the peak stress and the corresponding strain of the unconfined concrete cylinder specimen, respectively.

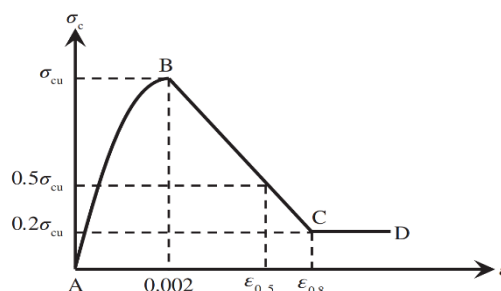


Figure 6. Concrete uniaxial compressive behavior [38]

The inelastic hardening strain in compression, $\epsilon_c^{in,h}$ can be calculated as follows:

$$\epsilon_c^{in,h} = \epsilon_c - \frac{\sigma_c}{E_c} \tag{2}$$

where E_c is the concrete modulus of elasticity.

Concrete behavior is a complex phenomenon that is influenced by cyclic behavior and several effective parameters. Among these parameters, damage in compression and tension plays a crucial role in defining concrete behavior. The inelastic hardening strain in compression ($\epsilon_c^{in,h}$), which controls the unloading curve slope, determines compression damage, which is represented by the variable d_c . As the inelastic hardening strain increases, the compression damage also increases, according to Equation 3. Therefore, it is essential to consider these parameters when designing concrete structures to ensure their durability and safety.

$$d_c = 1 - \frac{\sigma_c}{\sigma_{cu}} \tag{3}$$

where d_c is the scalar compression damage variable.

Concrete tension is an important factor to consider when it comes to damage modeling. Two steps are involved in defining the tensile characteristics of concrete. The first step is the linear part, which is the elastic part that stops at the tensile strength of the concrete and begins at zero stress. The second step, known as tension stiffening, is the non-linear post-peak part. The stress-strain curve has been plotted using Equations 4 to 7 adopting the model proposed by Wang and Hsu [39].

$$\sigma_t = E_c \epsilon_t, \text{ for } \epsilon_t \leq \epsilon_{cr} \tag{4}$$

$$\sigma_t = f_{ct} \left(\frac{\epsilon_{cr}}{\epsilon_t} \right)^{0.4}, \text{ for } \epsilon_t > \epsilon_{cr} \tag{5}$$

$$\epsilon_{cr} = \frac{f_{ct}}{E_c} \tag{6}$$

$$d_t = 1 - \frac{\sigma_t}{f_{ct}} \tag{7}$$

where σ_t and ϵ_t are the nominal tensile stress and its corresponding strain, respectively. f_{ct} is the tensile strength for concrete. ϵ_{cr} is the concrete's cracking strain. d_t is the scalar tension damage variable.

The concrete modulus of elasticity, Poisson's ratio, the damage plasticity parameters, and the behaviour of concrete in both compression and tension are presented in Table 10.

Table 10. Compression and tension concrete characteristics

Material's parameters	$f'_c = 45.6$	Plasticity parameters	
		Dilation angle	40
Concrete elasticity		Eccentricity	0.1
E	31050	fb0/fc0	1.16
v	0.19	K	0.667
		Viscosity parameter	0.0008
Concrete Compressive Behavior		Concrete Compression Damage	
Yield stress (MPa)	Inelastic strain	Damage parameter C	Inelastic strain
0	0	0	0
16.73726	0.0000237	0	0.0000237
29.66366	0.00004456	0	0.00004456
37.26097	0.00019997	0	0.00019997
42.41934	0.00043384	0	0.00043384
45.13877	0.00074626	0	0.00074626
45.41924	0.00113722	0.003964	0.00113722
43.26078	0.00160674	0.051299	0.00160674
38.66337	0.0021548	0.152119	0.0021548
17.96969	0.00377127	0.605928	0.00377127
Concrete Tensile Behavior		Concrete Tension Damage	

Yield stress (MPa)	Cracking strain	Damage parameter T	Cracking strain
2	0	0	0
1.426201	0.000104068	0.28689932	0.000104068
1.271175	0.00015906	0.36441248	0.00015906
0.963371	0.000368974	0.51831474	0.000368974
0.819138	0.000573619	0.59043121	0.000573619
0.730098	0.000776486	0.63495083	0.000776486
0.667755	0.000978494	0.66612234	0.000978494
0.567781	0.001481714	0.7161095	0.001481714
0.1	0.001996779	0.95	0.001996779

By utilizing the classical elastic-plastic model with strain hardening for steel, this study has been able to achieve reliable and accurate results. However, it is imperative to provide the steel modulus elasticity, Poisson’s ratio, and the yield stress-plastic strain data in ABAQUS to define the model.

4.5. Concrete-Reinforcement Interaction

The ABAQUS software's "embedded region" function is a powerful tool that enables accurate simulations of the interaction between concrete and reinforcing bars. By assuming full composite action between the two materials, the function enables both linear and nonlinear analysis. Specifically, in this simulation, the reinforcing bars will be selected as the embedded parts, while the concrete will be selected as the host part. Utilizing "embedded region" in the analysis will help to achieve more precise and reliable results.

5. Numerical Modeling Verification

A number of factors were taken into account by the built-up finite element model in order to get a high degree of compatibility with the experimental results. These included the mechanical characteristics of the concrete, the tensile strength of the steel reinforcement, the condition of supports, and the procedure by which the applied load was generated. As shown in Table 10 and Figure 4, all of the necessary finite element analysis data matched the experimentally observed properties. The results of the experimentally tested specimen and the numerical model were compared in order to examine the validity of the developed FE model. Particularly at the elastic zone (before to crack formation), an agreement on the load-deflection relationship was reached (Figure 7). The variation in the crack load was 3% while it reached 6.5% for the ultimate load. An acceptable level of convergence was indicated by the greatest errors for the deflection under cracking and ultimate loads, which were 4.2% and 5.7%, respectively. The evaluation of the developed model process also took the crack pattern into account. The developed crack pattern for the numerical and experimental instances showed good agreement (Figure 8). Finite element analysis's assumptions, particularly those pertaining to the interaction phenomena between the concrete and reinforcing bars, account for the difference between the experimental and numerical results. Furthermore, although concrete is entirely heterogeneous, it is regarded as a homogeneous material in finite element modelling.

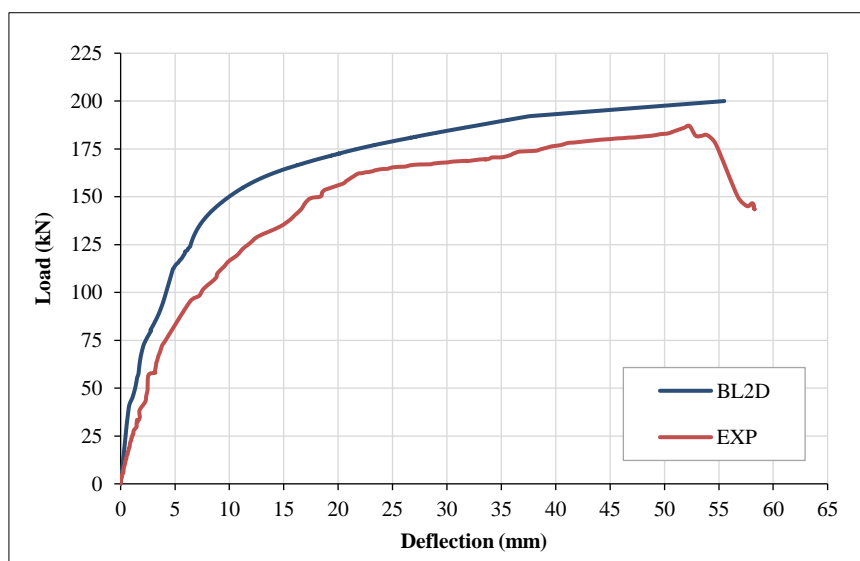


Figure 7. Load-deflection relation for the experimental and numerical test

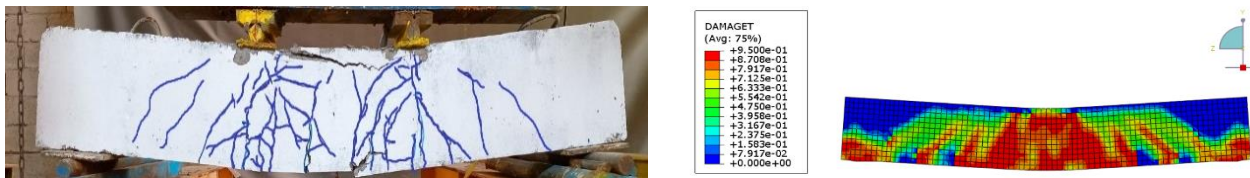


Figure 8. Crack pattern for the experimental and numerical test

6. Numerical Analysis Results

To achieve an accurate and significant investigation concerning the lacing reinforcement arrangement's influence on the structural behavior of deep reinforced concrete beams, several structural properties were included in the analysis, comprising crack load, ultimate load, load-deflection relation, stiffness, flexural toughness, ductility index, and load-strain relation for the flexural and shear reinforcement.

The findings showed that all of the lacing reinforcement schemes proposed in this study enhanced the cracking load in comparison to the conventional shear stirrups utilized in the specimen (BNS). The cracking load was significantly increased by the lacing reinforcement with a phase difference equal to the half-lacing cycle that was used in beams (BL2D) and (BL2S1D) as opposed to the lacing reinforcement without phase changes that was used in beams (BL2S) and (BL3S). In contrast to the specimen's (BNS) cracking load, the enhancement for the specimens (BL2D and BL2S1D) was 100% and 113.3%, respectively. While it was 6.7% and 27.1% for the specimens (BL2S) and (BL3S), respectively. Additionally, the specimens (BL2D), (BL2S), (BL2S1D), and (BL3S) demonstrated the benefit of the lacing reinforcement with a phase difference equivalent to the half-lacing cycle by their ultimate load results. 16.75% and 27.62% improvements were obtained when comparing (BL2D) with (BL2S) and (BL2S1D) with (BL3S), respectively. This is due to the fact that the layers of opposite lacing reinforcement function inside the concrete member like a truss action, which is incredibly effective in a variety of directions. This enhances the loading distribution and increases the shear resistance capacity, delaying the formation of shear cracks while preserving the structural integrity of the entire structural member.

Table 11 illustrates the lacing effect with regard to cracking, service, yielding, ultimate load, and deflection for the four suggested lacing arrangements, while Table 12 shows the lacing advantages over the specimen (BNS) with two-legged steel stirrups. For the same net shear reinforcement cross-sectional area, another significant finding was found with reference to the number of lacing bars. Obviously, in the case of a similar lacing phase, as seen in Table 11, increasing the number of lacing bars from two to three moderately increased the specimen strength, as long as the shear reinforcement area was maintained. The specimen (BL3S) had a service, yielding, and ultimate load that was 2.40%–2.96% higher than the specimen (BL2S). This was not completely applicable to the cracking load, where the difference was 14.4%.

Table 11. Load and deflection at different loading stages

Beam Designation	First flexure cracking load		Service stage		Yielding stage		Ultimate stage		Stiffness <i>K</i> kN/mm	Ductility Index μ
	P_{cr} (kN)	Δ_{cr} (mm)	$P_{service}$ (kN)	$\Delta_{service}$ (mm)	P_y (kN)	Δ_y (mm)	P_u (kN)	Δ_u (mm)		
BNS	22.5	0.85	99.5	4.5	106.6	8.4	153.1	49.2	26.5	5.9
BL2D	45.0	1.09	130.0	6.8	128.8	6.7	200.0	55.5	41.3	8.3
BL2S	25.0	0.85	111.3	8.4	116.5	8.8	171.3	50.0	29.4	5.6
BL2S1D	48.0	1.16	146.3	6.4	133.5	5.3	225.0	60.2	41.4	11.4
BL3S	28.6	0.90	114.6	9.0	119.3	9.1	176.3	52.1	31.8	5.7

Table 12. Enhancement due to the lacing reinforcement arrangement

Beam Designation	Enhancement (%)					
	P_{cr}	$P_{service}$	P_y	P_u	<i>K</i>	μ
BNS	---	---	---	---	---	---
BL2D	100	30.7	20.8	30.6	55.85	40.68
BL2S	6.7	11.9	9.3	11.9	10.94	-5.08
BL2S1D	113.3	47.0	25.2	47.0	56.23	93.22
BL3S	27.1	15.2	11.9	15.2	20.0	-3.39

The number of lacing bars had a greater impact on lacing reinforcement when the phase difference was equivalent to the half-lacing cycle. Compared to BL2D, the specimen (BL2S1D) exhibited superior resistance to cracking, service, yielding, and failure loads. The enhancement level for this resistance varied from 3.6% to 12.5%, with the lacing bar number having a greater effect on the final strength of the beam.

Three stages were seen in the load-deflection graphs (Figure 9). The elastic zone where the analyzed specimens were divided into two groups is described in the first stage. Table 11 and Figure 10 demonstrate that the lacing reinforcement and its arrangement in the first group of specimens (BL2S and BL3S) did not effectively increase the specimen stiffness. In comparison to (BNS), the stiffness of (BL2S) and (BL3S) improved by 10.94% and 20%, respectively. The impact of the lacing reinforcement arrangement was entirely different in the second group of specimens (BL2D and BL2S1D), where the stiffness increased by almost 56% in comparison to the specimen (BNS).

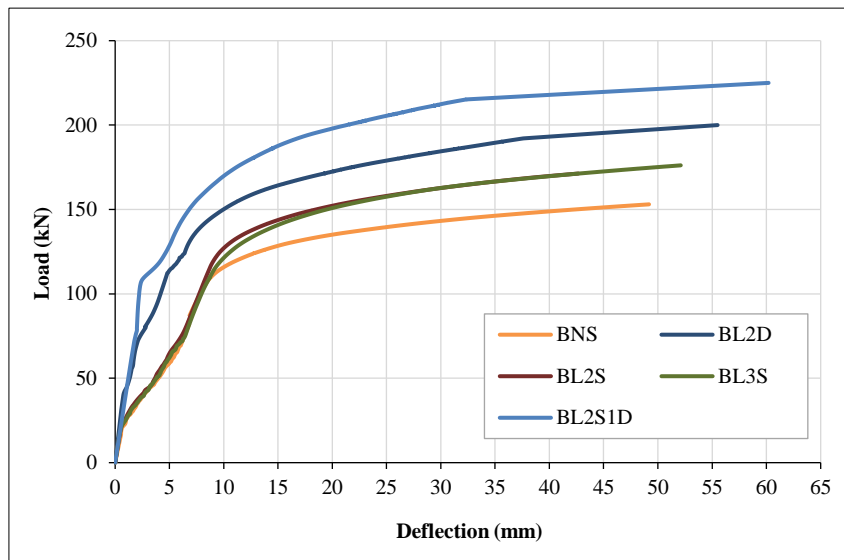


Figure 9. Load-deflection relation for the considered parameters

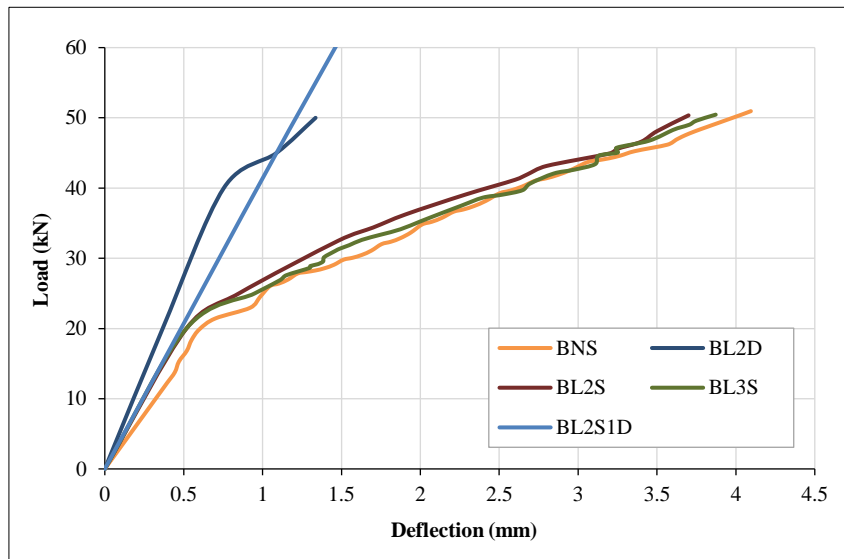


Figure 10. Elastic load-deflection relation for the considered parameters

Comparable behavior to the first stage was noted in the second stage, which continued until the yielding level. Every specimen's deflection curve diverged when the nonlinear response became valid (third stage), with the exception of specimens BL2S and BL3S. The best response was shown by specimen (BL2S1D), followed by specimen (BL2D), and the weakest was shown by specimen (BNS).

Using lacing reinforcement with a phase difference equal to the half-lacing cycle as presented in beams (BL2D) and (BL2S1D) considerably increased the ductility index compared to the conventional shear stirrups utilized in the specimen (BNS). The enhancement was 40.68% and 93.22% for specimens (BL2D) and (BL2S1D), respectively.

Otherwise, in comparison to the specimen (BNS), the effect on the ductility index was negligible when shear lacing bars was utilized without phase lag. A slight reduction was noticed in the ductility index of the specimens (BL2S) and (BL3S) of 5.08% and 3.39%, respectively.

One of the most important indicators in assessing the structural performance is flexural toughness, also known as absorbed energy capacity. Flexural toughness was calculated by integrating the area under the load-deflection or stress-strain curve [40-42]. In order to better understand the structural behavior of laced reinforced concrete deep beams, four load levels were included in the investigation of flexural toughness: first flexure cracking load, service load, yielding load, and ultimate load. According to Tables 13 and 14, the results show the same response in each of the loading stages that were investigated.

Table 13. Flexural toughness at different loading stages

Beam Designation	Flexural toughness, (kN.mm)			
	First flexure cracking load	Service load	Yielding load	Ultimate load
BNS	13.34	408.879	462.23	6165.61
BL2D	37.86	578.22	566.22	9470.31
BL2S	18.66	501.72	543.02	7140.63
BL2S1D	41.84	641.97	580.84	11903.50
BL3S	21.65	560.92	551.86	7391.61

Table 14. Enhancement of the flexural toughness

Beam Designation	Enhancement (%)			
	First flexure cracking load	Service load	Yielding load	Ultimate load
BNS	---	---	---	---
BL2D	183.81	41.42	22.50	53.60
BL2S	39.88	22.71	17.48	15.81
BL2S1D	213.64	57.01	25.66	93.06
BL3S	99.18	37.18	19.39	19.88

In the cracking and ultimate stages, where the specimen (BL2S1D) demonstrated the greatest improvement of 213.64% and 93.06%, respectively, the flexural toughness was improved by replacing lacing reinforcement for conventional two-legged steel stirrups. With the same net shear reinforcement cross-sectional area, flexural toughness increased as the number of lacing reinforcing bars increased. The effect was more pronounced up to the yielding load, so the improvement for specimen (BL3S) compared to specimen (BL2S) was 16.02% and 11.8%, while the improvement for specimen (BL2S1D) compared to specimen (BL2D) was 10.51% and 11.03% with regard to the first flexure cracking load and service load, respectively. However, at the yielding and ultimate loads, the improvement occasionally proved insignificant. When comparing specimens (BL3S) and (BL2S), it was 1.63% and 3.51%, respectively, and when comparing specimens (BL2S1D) and (BL2D), it was 2.58% and 25.69%.

Furthermore, among the factors that were taken into consideration, the lacing reinforcement with a phase difference equal to the half-lacing cycle has the largest impact. According to a comparison between the specimens (BL2S) and (BL2D) and (BL3S) and (BL2S1D), which represent the cases of two and three lacing bars with identical shear reinforcement cross-sectional areas, respectively, the enhancement level of the first flexure cracking load reached 102.90% and 93.26%, while the ultimate load was 32.63% and 61.04%.

Figure 11 and Table 15 present the results of the strain that was measured or calculated in the longitudinal reinforcement. The load-strain relationship showed the same result for the parameters under consideration. After the yielding stage, the analyzed specimens with lacing reinforcement with a phase difference equivalent to the half-lacing cycle (BL2D and BL2S1D) became distinguished from those with lacing reinforcement without phase changes and two-legged steel stirrups (BNS, BL2S, and BL3S), reflecting the stiffened behavior offered by the phase lag arrangement of the lacing reinforcement. The strain-load relationship for the shear reinforcement is

shown in Figure 12, and it is evident that the phase lag arrangement of the lacing reinforcement significantly impacted the overall beam response. In specimens BL2D and BL2S1D, the produced strain was greater than in specimens BNS, BL2S, and BL3S; in other words, the contribution of lacing reinforcement to the beam strength increased.

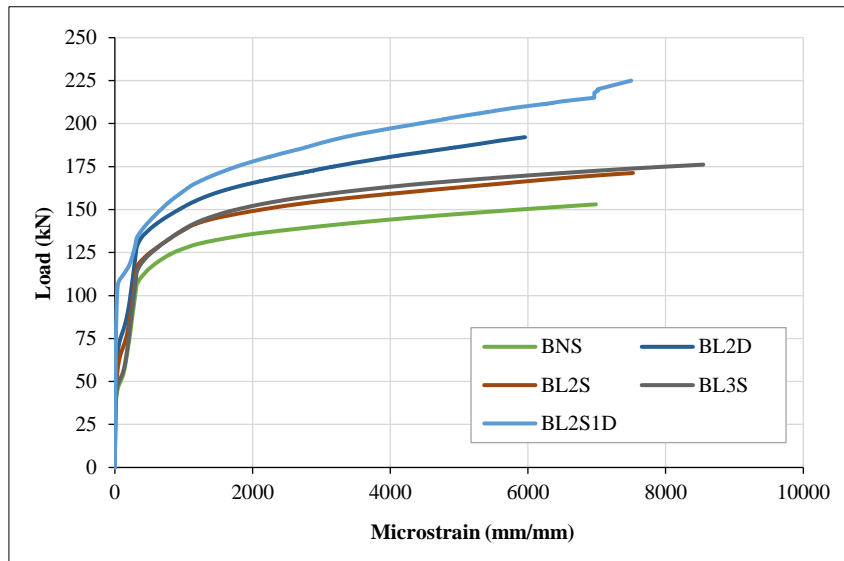


Figure 11. Load-flexural strain relation for the considered parameters

Table 15. Maximum strain in flexural and shear reinforcement at ultimate load

Beam Designation	Max. Strain $\mu\epsilon$ (mm/mm)	
	Flexural Reinforcement	Shear Reinforcement
BNS	6986	1438
BL2D	6000	2500
BL2S	7526	2598
BL2S1D	7500	4519
BL3S	8546	3548

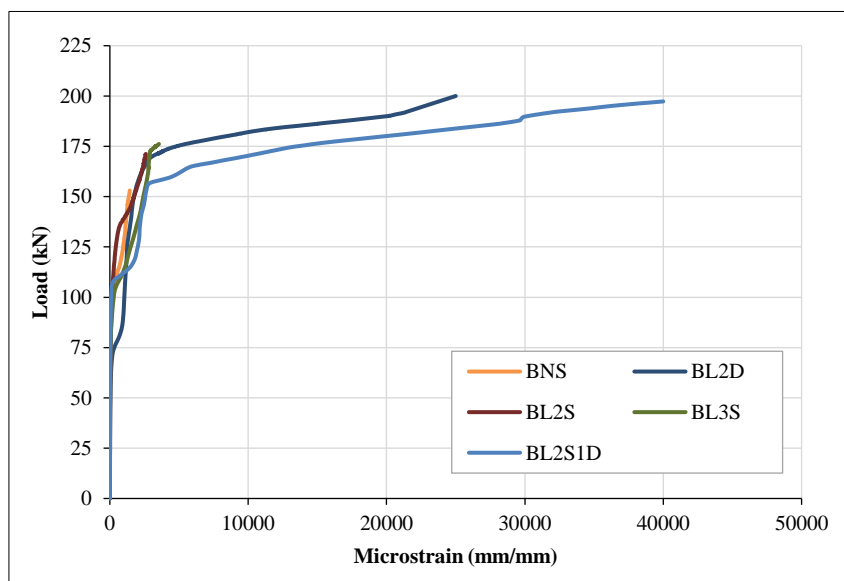


Figure 12. Load-shear strain relation for the considered parameters

It is evident from a comparison of the shear and flexural reinforcement shown in Figure 13 that the lacing reinforcement strain progressed at a faster rate after the flexural reinforcement yielding stage. This only applied in the case of the phase lag arrangement; in the other instance, the strain-increasing rate was still constrained.

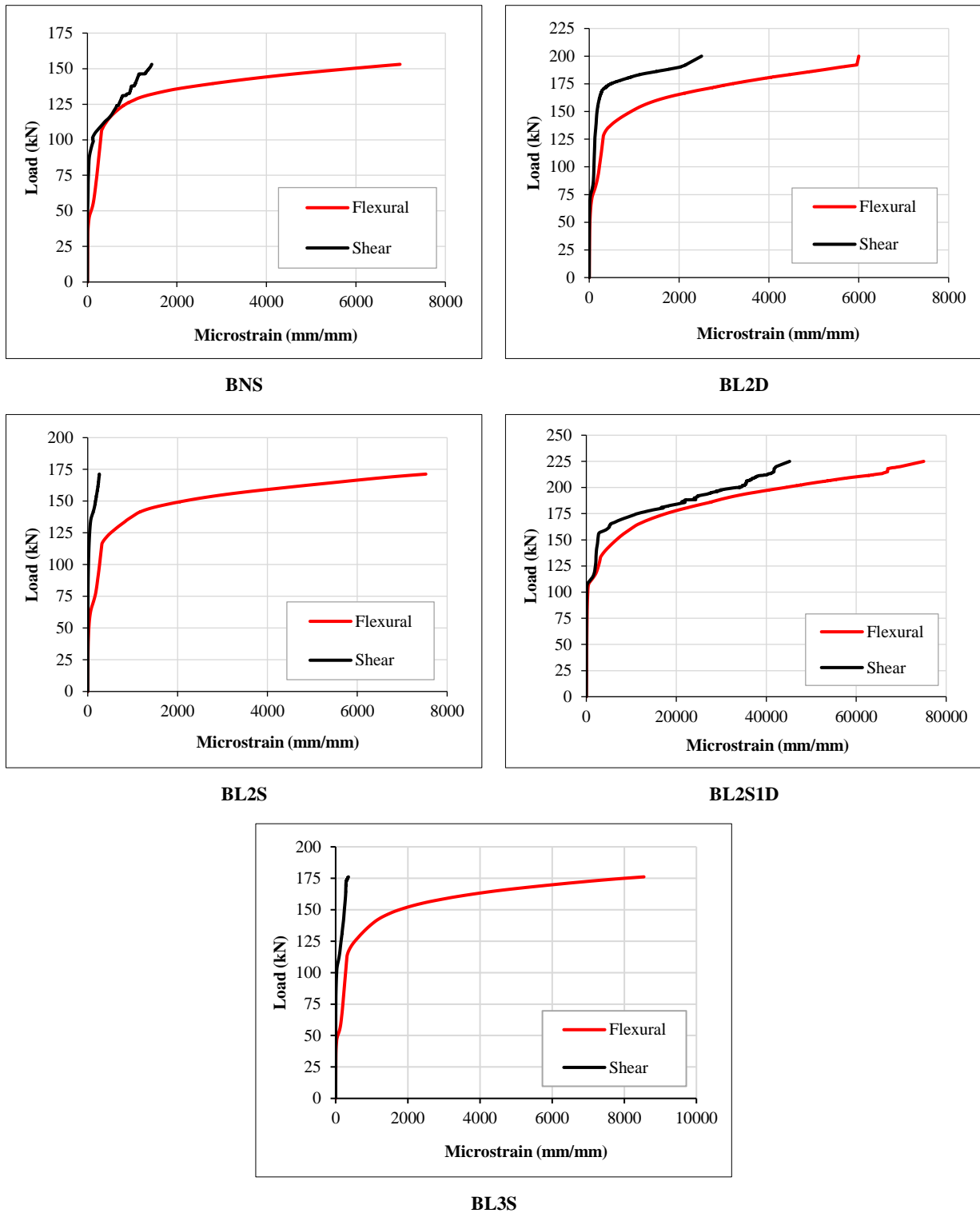


Figure 13. Flexural and shear strain for the considered parameters

Figure 14 illustrates the failure mode for the specimen that was subjected to numerical analysis. Each specimen exhibited a shear crack that began at the support locations and progressed toward the applied load, in addition to a flexural mode of failure. Table 16 shows that the analyzed specimens had varying recorded first shear cracking loads. The first shear cracking stress of all the laced reinforced specimens was higher than that of conventional shear stirrups. Specimens with lacing reinforcement of phase lag arrangement (BL2D) and (BL2S1D) showed the greatest improvement compared to specimen (BNS), reaching 92.44% and 217.07%, respectively, while specimens with lacing reinforcement without phase lag arrangement (BL2S) and (BL3S) showed the least improvement, at 36.91% and 46.53%, respectively.

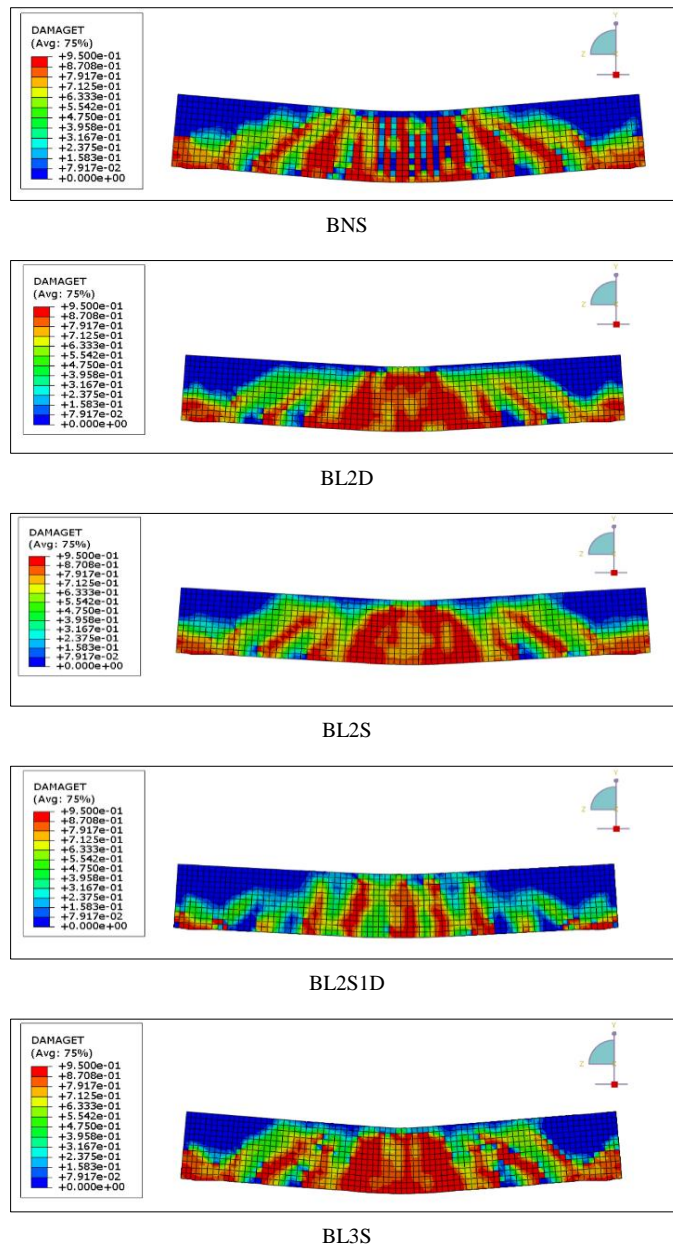


Figure 14. Crack pattern for the considered parameters

Table 16. Generated first shear cracking load

Beam Designation	P_{cr} (kN)	Enhancement (%)
BNS	37.44	---
BL2D	72.05	92.44
BL2S	51.26	36.91
BL2S1D	118.71	217.07
BL3S	54.86	46.53

The lacing reinforcement's noticeable activity in resisting the diagonal tension stress, as compared to the vertical shear reinforcement, was the main reason for the improved shear strength. This beneficial effect is frequently caused by the lacing reinforcement's inclined orientation, which is almost perpendicular to the shear cracks that occur.

If the number of lacing bars were increased while keeping the net shear reinforcement cross-sectional area consistent, it would be more worthwhile to look into. An additional case study was taken into consideration for this reason, showing four bars arranged similarly to those in specimens (BL2S) and (BL3S) (see Figure 15).

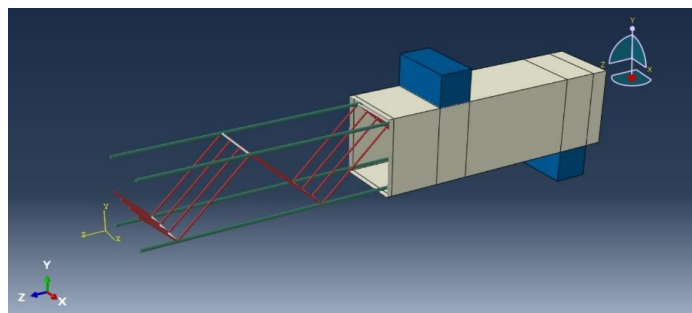


Figure 15. Finite element model for 4-lacing bars of the same arrangement

The results of the FE analysis, which included the failure mode, ultimate load, yielding load, first cracking load, first shear cracking load, stiffness, and ductility index, showed that adding more lacing bars while keeping the net shear reinforcement cross-sectional area constant did not always have a favorable impact. As seen in Figure 16 and Table 17, a lower level of overall response of the specimen was noted when four lacing bars were considered as an alternative to the case of two lacing bars. However, as Figure 17 illustrates, the failure mode remained the same. This is explained by the fact that the reduction in steel bar diameter has a major impact on several aspects of the structural members, including stiffness, deformation, and overall strength.

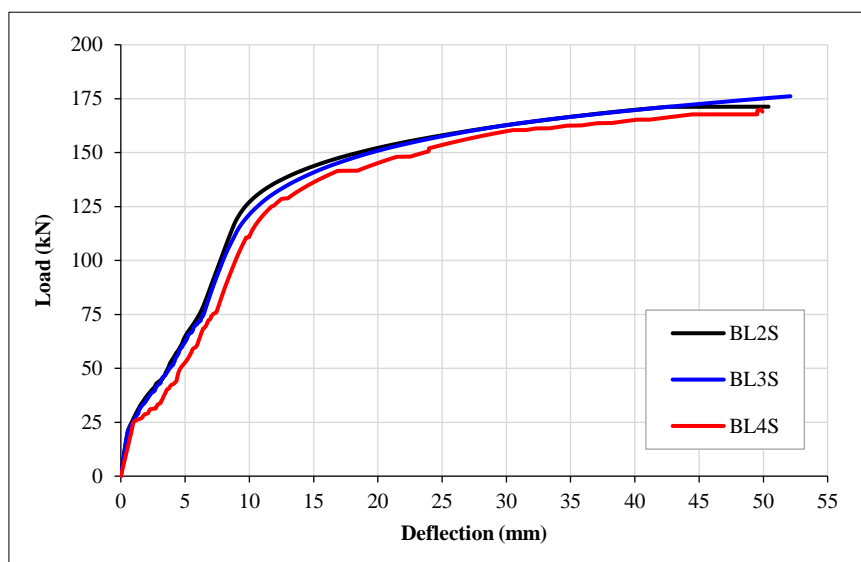


Figure 16. Load-deflection relation for the lacing bar numbers effect

Table 17. Summary of the lacing bar numbers effect

Beam Designation	First flexure cracking load		First shear cracking load		Yielding load		Ultimate load		Stiffness K (kN/mm)	Ductility index μ
	P_{cr} (kN)	Δ_{cr} (mm)	P_{cr} (kN)	Δ_{cr} (mm)	P_y (kN)	Δ_y (mm)	P_u (kN)	Δ_u (mm)		
BL2S	25.0	0.85	51.3	4.1	116.5	8.8	171.3	50.0	29.4	5.6
BL3S	28.6	0.90	54.9	4.0	119.3	9.1	176.3	52.1	31.8	5.7
BL4S	24.4	0.90	50.1	4.9	114.7	9.5	170.5	49.8	27.1	5.2

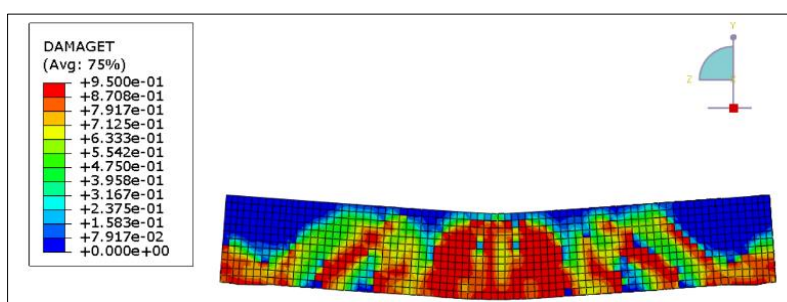


Figure 17. Crack pattern for 4-lacing bars of the same arrangement

7. Conclusion

The impact of three parameters—the type of shear reinforcement, the number of lacing bars that maintain a constant net shear reinforcement cross-sectional area, and the lacing arrangement (phase lag)—was explored in a validated Finite Element Model for a reinforced concrete deep beam transversely reinforced with lacing bars. Many findings were detected based on the results of the numerical analysis. In comparison to the conventional vertical stirrups, lacing reinforcement improved the deep beam's overall performance, including cracking load, ultimate load, stiffness, ductility index, and flexural toughness, regardless of the lacing arrangement and number of bars. The findings of the theoretical study demonstrated that the type of arrangement significantly influences the deep beam structural response with regard to the lacing arrangement under consideration (i.e., lacing reinforcement with a phase difference equal to the half-lacing cycle and lacing reinforcement without phase variations). The structural response was shown to be more enhanced by lacing reinforcement with a phase difference equivalent to the half-lacing cycle than by lacing reinforcement without a phase change. The results indicate that the type and arrangement of shear reinforcement had a greater influence than the number of lacing reinforcement bars used (for the same cross-sectional area). Furthermore, this effect changed as the number of lacing bars grew to four because of the effect of the bar diameter being reduced. This had a major influence on the strength, stiffness, and deformation of the structural element.

The use of lacing reinforcement also had an impact on shear cracking load; independent of the arrangement status and number of lacing bars, the first shear cracking load was higher than that of conventional shear stirrups.

8. Declarations

8.1. Author Contributions

Conceptualization, S.D. and H.M.; methodology, S.D. and N.O.; software, H.M. and T.H.; validation, S.D., A.A., and H.M.; formal analysis, S.D. and A.A.; investigation, S.D., N.O., A.A., and T.H.; resources, M.M.; data curation, S.D.; writing—original draft preparation, S.D.; writing—review and editing, N.O.; visualization, H.M.; supervision, N.O. and A.A.; project administration, S.D.; funding acquisition, S.D., A.A., and T.H. All authors have read and agreed to the published version of the manuscript.

8.2. Data Availability Statement

The data presented in this study are available on request from the corresponding author.

8.3. Funding

The authors received no financial support for the research, authorship, and/or publication of this article.

8.4. Acknowledgements

Thanks and appreciation are presented to the Structural Laboratory staff in the Department of Civil Engineering, University of Baghdad, Iraq for their support. The authors are also grateful to the Engineering Consulting Bureau at the University of Baghdad (CEB-UB) who contributed to completing the material testing.

8.5. Conflicts of Interest

The authors declare no conflict of interest.

9. References

- [1] Słowik, M. (2014). Shear Failure Mechanism in Concrete Beams. *Procedia Materials Science*, 3(2211–8128), 1977–1982. doi:10.1016/j.mspro.2014.06.318.
- [2] Yang, K. H., & Ashour, A. (2007). Tests on reinforced concrete deep beams. *Concrete (London)*, 41(1), 42–44. doi:10.14359/10558.
- [3] Saleh, M., AlHamaydeh, M., & Zakaria, M. (2023). Finite element analysis of reinforced concrete deep beams with square web openings using damage plasticity model. *Engineering Structures*, 278, 115496. doi:10.1016/j.engstruct.2022.115496.
- [4] Allawi, A. A., Oukaili, N. K., & Jasim, W. A. (2021). Strength compensation of deep beams with large web openings using carbon fiber-reinforced polymer sheets. *Advances in Structural Engineering*, 24(1), 165–182. doi:10.1177/1369433220947195.
- [5] M. Mhalhal, J., S. Al-Gasham, T., & A. Jabir, H. (2018). New Technique to Enhance the Shear Performance of RC Deep Beams Using Mild Steel Plates. *International Journal of Engineering & Technology*, 7(4.20), 86. doi:10.14419/ijet.v7i4.20.25854.
- [6] Woodson, S. C. (1992). Lacing versus stirrups: An experimental study of shear reinforcement in blast-resistant structures. Waterways Experiment Station, Structures Laboratory, US Army Corps of Engineers, Washington, United States.

- [7] Fan, S., Zhang, Y., & Tan, K. H. (2022). Fire behaviour of deep beams under unsymmetrical loading. *Engineering Structures*, 250, 113419. doi:10.1016/j.engstruct.2021.113419.
- [8] Campione, G., & Minafò, G. (2012). Behaviour of concrete deep beams with openings and low shear span-to-depth ratio. *Engineering Structures*, 41, 294-306. doi:10.1016/j.engstruct.2012.03.055.
- [9] Fan, S., Tan, K. H., & Nguyen, M. P. (2018). Numerical model to determine shear capacity of reinforced concrete deep beams exposed to fire. *Fib Symposium*, 1410–1419. doi:10.1007/978-3-319-59471-2_162.
- [10] Kareem, A., & Mohammed, S. D. (2023). The Experimental and Theoretical Effect of Fire on the Structural Behavior of Laced Reinforced Concrete Deep Beams. *Engineering, Technology and Applied Science Research*, 13(5), 11795–11800. doi:10.48084/etasr.6272.
- [11] Ali Al-Tameemi, S. K., Al-hasany, E. G., Mohammad, H. K., Jabir, H. A., Ibrahim, T. H., Allawi, A. A., & El-Zohairy, A. (2024). Simulation and design model for reinforced concrete slabs with lacing systems. *Advances in Structural Engineering*, 27(5), 871–892. doi:10.1177/13694332241237576.
- [12] Al-Ghrery, K., Al-Mahaidi, R., Kalfat, R., Oukaili, N., & Al-Mosawe, A. (2021). Experimental Investigation of Curved-Soffit RC Bridge Girders Strengthened in Flexure Using CFRP Composites. *Journal of Bridge Engineering*, 26(4), 04021009. doi:10.1061/(asce)be.1943-5592.0001691.
- [13] Anandavalli, N., Lakshmanan, N., Iyer, N. R., Prakash, A., Ramanjaneyulu, K., Rajasankar, J., & Rajagopal, C. (2012). Behaviour of a blast loaded laced reinforced concrete structure. *Defence Science Journal*, 62(5), 284–289. doi:10.14429/dsj.62.820.
- [14] Anandavalli, N., Lakshmanan, N., Prakash, A., Rajasankar, J., & Iyer, N. R. (2015). Numerical Investigations on a Blast Loaded Laced Reinforced Concrete Structure using an Equivalent Constitutive Property. *Journal of The Institution of Engineers (India): Series A*, 96(4), 311–318. doi:10.1007/s40030-015-0139-6.
- [15] Anandavalli, N., Lakshmanan, N., Knight, G. S., Iyer, N. R., & Rajasankar, J. (2012). Performance of laced steel–concrete composite (LSCC) beams under monotonic loading. *Engineering Structures*, 41, 177-185. doi:10.1016/j.engstruct.2012.03.033.
- [16] Park, R., & Ruitong, D. (1988). Ductility of Doubly Reinforced Concrete Beam Sections. *ACI Structural Journal*, 85(2), 217–225. doi:10.14359/2760.
- [17] Ismael, T. M., & Mohammed, S. D. (2021). Structural performance of fiber-reinforced lightweight concrete slabs with expanded clay aggregate. *Materials Today: Proceedings*, 42(4), 2901–2908. doi:10.1016/j.matpr.2020.12.746.
- [18] Adnan Hadi, M., & Mohammed, S. D. (2021). Improving torsional - Flexural resistance of concrete beams reinforced by hooked and straight steel fibers. *Materials Today: Proceedings*, 42, 3072–3082. doi:10.1016/j.matpr.2020.12.1046.
- [19] Poongodi, K., Murthi, P., & Gobinath, R. (2020). Evaluation of ductility index enhancement level of banana fibre reinforced lightweight self-compacting concrete beam. *Materials Today: Proceedings*, 39(1), 131–136. doi:10.1016/j.matpr.2020.06.397.
- [20] Seleem, M. H., Megahed, F. A., Badawy, A. A. M., & Sharaky, I. A. (2023). Performance of NSM and EB methods on the flexural capacity of the RC beams strengthened with reinforced HSC layers. *Structures*, 56, 104950. doi:10.1016/j.istruc.2023.104950
- [21] Maghsoudi, A. A., & Akbarzadeh Bengar, H. (2006). Flexural ductility of HSC members. *Structural Engineering and Mechanics*, 24(2), 195–212. doi:10.12989/sem.2006.24.2.195.
- [22] Al-Gasham, T. S., Mhalhal, J. M., & Abid, S. R. (2020). Flexural Behavior of Laced Reinforced Concrete Moderately Deep Beams. *Case Studies in Construction Materials*, 13, e00363. doi:10.1016/j.cscm.2020.e00363.
- [23] Lakshmanan, N. (2008). Laced reinforced concrete construction technique for blast resistant design of structures. *Proceedings of the Sixth Structural Engineering Convention*, 18-20 December, 2008, Chennai, India.
- [24] Allawi, A. A., & Jabir, H. A. (2016). Experimental Behavior of Laced Reinforced Concrete One Way Slab under Static Load. *Journal of Engineering*, 22(5), 42–59. doi:10.31026/j.eng.2016.05.04.
- [25] Hallawi, A. F., & Al-Ahmed, A. H. A. (2019). Enhancing the Behavior of One-Way Reinforced Concrete Slabs by Using Laced Reinforcement. *Civil Engineering Journal (Iran)*, 5(3), 718–728. doi:10.28991/cej-2019-03091282.
- [26] Abdullah, A. I., & Al-Khazraji, S. D. M. (2019). Structural Behavior of High Strength Laced Reinforced Concrete One Way Slab Exposed to Fire Flame. *Civil Engineering Journal (Iran)*, 5(12), 2747–2761. doi:10.28991/cej-2019-03091446.
- [27] Abdullah, M., Nakamura, H., & Miura, T. (2024). Experimental investigation on influence of vertical stirrup legs to shear failure behavior in RC beams. *Developments in the Built Environment*, 18(100451). doi:10.1016/j.dibe.2024.100451.
- [28] Johnson, B. G. C., Ramasamy, M., & Narayanan, A. (2024). Experimental study and assessment of the structural performance of laced reinforced concrete beams against reverse cyclic loading. *Matéria (Rio de Janeiro)*, 29(1), e20240001. doi:10.1590/1517-7076-rmat-2024-0001.

- [29] Bello, B.R., & Dela Cruz, O.G. (2024). Shear and Flexural Performance of Reinforced Concrete Beams with Modified Shear Reinforcement: A Literature Review. *Proceedings of the International Conference on Geosynthetics and Environmental Engineering, ICGEE 2023, Lecture Notes in Civil Engineering*, 374, Springer, Singapore. doi:10.1007/978-981-99-4229-9_9.
- [30] Bello, B. R., Dela Cruz, O. G., Muhi, M. M., & Guades, E. J. (2024). Enhancing the Flexural Capacity of Reinforced Concrete Beam by Using Modified Shear Reinforcement. *Civil Engineering Journal (Iran)*, 10(6), 1720–1741. doi:10.28991/CEJ-2024-010-06-02.
- [31] Iraqi Specification No. 5. (2019). Portland Cement. Central Agency for Standardization and Quality Control, Baghdad, Iraq.
- [32] Iraqi Specification No. 45. (1984). Aggregate from Natural Sources for Concrete and Construction. Central Organization for Standardization and Quality Control, Baghdad, Iraq.
- [33] ASTM C1240-20. (2020). Standard Specification for Silica Fume Used in Cementitious Mixtures. ASTM International, Pennsylvania, United States. doi:10.1520/C1240-20.
- [34] ASTM C494/C494M-17. (2020). Standard Specification for Chemical Admixtures for Concrete. ASTM International, Pennsylvania, United States. doi:10.1520/C0494_C0494M-17.
- [35] ASTM A615/A615M-05a. (2017). Standard Specification for Deformed and Plain Carbon-Steel Bars for Concrete Reinforcement. ASTM International, Pennsylvania, United States. doi:10.1520/A0615_A0615M-05A.
- [36] EFNARC. (2005). European Guidelines for Self-Compacting Concrete (SCC). EFNARC, FLUMS, Switzerland.
- [37] Coronado, C. A., & Lopez, M. M. (2006). Sensitivity analysis of reinforced concrete beams strengthened with FRP laminates. *Cement and Concrete Composites*, 28(1), 102–114. doi:10.1016/j.cemconcomp.2005.07.005.
- [38] Kent, D. C., & Park, R. (1971). Flexural Members with Confined Concrete. *Journal of the Structural Division*, 97(7), 1969–1990. doi:10.1061/jsdeag.0002957.
- [39] Wang, T., & Hsu, T. T. C. (2001). Nonlinear finite element analysis of concrete structures using new constitutive models. *Computers & Structures*, 79(32), 2781–2791. doi:10.1016/S0045-7949(01)00157-2.
- [40] Soboyejo, W. (2002). *Mechanical properties of engineered materials*. CRC Press, New York, United States. doi:10.1201/9780203910399.
- [41] Aslani, F., & Samali, B. (2014). Flexural toughness characteristics of self-compacting concrete incorporating steel and polypropylene fibres. *Australian Journal of Structural Engineering*, 15(3), 269–286. doi:10.7158/S13-011.2014.15.3.
- [42] Allawi, A. A., Shubber, A. N., Al Gharawi, M., El-Zohairy, A., Ibrahim, T. H., Al-Ahmed, A. H. A., & Arafa, I. T. (2023). Enhancement of RC T-beams toughness using laced stirrups reinforcement for blast response predictions. *Structural Concrete*, 24(3), 3839–3856. doi:10.1002/suco.202200894.